Magnetic and magnetothermal properties, and the magnetic phase diagram of single-crystal holmium along the easy magnetization direction

2015 J. Phys.: Condens. Matter 27 146002

(http://iopscience.iop.org/0953-8984/27/14/146002)

IOP Publishing Journal of Physics: Condensed Matter
J. Phys.: Condens. Matter **27** (2015) 146002 (9pp) doi:10.1088/0953-8984/27/14/146002

Magnetic and magnetothermal properties, and the magnetic phase diagram of single-crystal holmium along the easy magnetization direction

V I Zverev[1,2], A M Tishin[1,3], Zou Min[4], Ya Mudryk[5], K A Gschneidner Jr[5,6] and V K Pecharsky[5,6]

[1] Faculty of Physics, M.V. Lomonosov Moscow State University, 119991, Moscow, Russia
[2] Pharmag LLC, 142190, Troitsk, Russia
[3] Advanced Magnetic Technologies and Consulting LLC, 142190, Troitsk, Russia
[4] Structural and Functional Metals Laboratory, Ceramic & Metallurgy Technologies, GE Global Research Center, 1 Research Circle, Niskayuna, NY 12309
[5] The Ames Laboratory US Department of Energy, Iowa State University, Ames, IA 50011-3020, USA
[6] Department of Materials Science and Engineering, Iowa State University, Ames, IA 50011-2300, USA

E-mail: vi.zverev@physics.msu.ru

Received 25 October 2014, revised 7 January 2015
Accepted for publication 23 February 2015
Published 19 March 2015

Abstract

The magnetic and magnetothermal properties of holmium single crystal have been investigated from 4.2 to 300 K in magnetic fields up to 100 kOe using magnetization and heat capacity data measured along the easy magnetization direction, which is the crystallographic *b*-axis, i.e. [1 1 $\bar{2}$ 0] direction. The magnetic phase diagram of Ho has been refined by examining data measured using a high purity single crystal.

Keywords: lanthanide metals, holmium single crystal, phase diagram

(Some figures may appear in colour only in the online journal)

1. Introduction

Experimental investigations of the magnetic properties and structures of heavy lanthanides, including Ho, began in the 1950s. Holmium has one of the largest magnetic moments in the lanthanide series, $\mu_{\text{eff}} = 10.61\,\mu_{\text{B}}$ [1]. The metal exhibits numerous magnetic phase transitions as the temperature and/or magnetic field vary. At low temperatures a paramagnetic (PM) to antiferromagnetic (AFM) transition occurs at ~133 K in a polycrystalline sample, and a second, apparently ferromagnetic (FM) transition, around 20 K [2]. A pronounced anisotropy of the magnetization has been observed in single-crystalline Ho in the basal plane [3].

Thermal measurements of polycrystalline Ho have revealed two distinct peaks in the temperature dependence of specific heat: a strong λ-type anomaly that peaks at 131.6 K and a weaker, history-dependent peak that is found at 19.4 K [4]. Neutron-diffraction measurements from room temperature down to 4.2 K have been made on single-crystal samples of Ho by Koehler *et al* [5]. Below 20 K the structure is conical in which there is a net moment of 1.7 μ_{B} parallel to the *c*-axis. Neutron-diffraction measurements in applied magnetic fields up to 22.3 kOe [6], showed that at low temperatures the *b*-direction is the easy magnetization axis. A schematic phase diagram constructed in [8] shows a number of magnetic phase transitions (at that moment, mainly of the unknown origin) over the field–temperature landscape.

Akhavan and Blackstead [7] reported magnetoresistance measurements on single crystals for the helical antiferromagnetic and conical ferromagnetic phases, refined the phase diagram, and proved the existence of an additional stable intermediate state.

In the 1980s a number of new magnetic structures of Ho, such as the spin–slip phases and the helifans, were discovered [8]. Ali *et al* [9] have observed anomalies in the temperature dependence of the magnetization at 21, 42, and 98 K and

that was, as far as we know, the first and the only time these spin–slip transitions have been detected using magnetization measurements. The theoretical study by Hughes *et al* [10] summed up the experimental results and the authors noted that the trend from ferromagnetism to incommensurate ordering in the lanthanide series as atomic number increases is connected with the decrease in unit cell volume.

A number of authors have proposed magnetic phase diagrams for Ho [6, 7, 11], but significant differences are noted. In part this is due to using samples of different quality and, often, low purity, making it difficult to compare and, therefore, understand the nature of multiple phase transitions known to occur in elemental Ho. Further, since magnetic phase transitions in rare earth metals may be strongly affected by interstitial impurities [12], the concentrations of which are often unreported, a systematic study of high-purity single crystal is of fundamental importance.

Here we report dc magnetization and heat capacity, all measured as functions of temperature and magnetic field using identical high-purity Ho crystals with the magnetic field applied parallel to the *b*-direction (i.e. [1 1 $\bar{2}$ 0] crystallographic direction, which coincides with the easy magnetization axis). The resultant magnetic phase diagram exhibits several additional features and phases that have not been reported previously, likely due to less pure samples that were employed in earlier studies.

2. Experimental details

The Ho single crystal investigated in this work was prepared by the Materials Preparation Center at the Ames Laboratory [13]. The major impurities in the polycrystalline metal, used to grow the single crystal by means of the strain-anneal process [14], were as follows (in ppm atomic): O, 239; H, 327; C, 123; F, 26; Fe, 32; N, 35; Ni, 11; and Cu, 9. Thus, the starting material was approximately 99.92 at.% (99.993 wt%) pure. The material had a residual resistivity ratio (RRR) of 160; the best RRR values reported in the previous investigations were 80–90. Crystallographic directions were determined using the back reflection Laue technique. The combined accuracy of the alignment of the crystallographic axes with the direction of the magnetic field vector was $\pm 5^{\circ}$.

The sample for the dc magnetization measurements was cut by using the spark-eroding technique from a large grain and shaped as parallelepiped with the approximate dimensions $1.57 \times 0.9 \times 0.59\,\mathrm{mm}^3$ (mass 4.6 mg). The longest dimension of the parallelepiped was parallel to the *b*-crystallographic axis of Ho (the easy magnetization direction). The sample for heat capacity measurements was a $9.52 \times 6.02 \times 2.8\,\mathrm{mm}^3$ parallelepiped weighing 1.3909 g. This heat capacity sample was used in the low field measurements from 0 to 40 kOe. The *b*-crystallographic axis of Ho was perpendicular to the sample plane and parallel to the magnetic field vector. After these measurements were completed the sample was cut to avoid excessive twisting of the sample holder due to the high magnetic moment of Ho in the heat capacity measurements in higher fields (50–100 kOe). The dimensions of the second sample were $6.17 \times 6.02 \times 2.52\,\mathrm{mm}^3$ and it weighed 0.8081 g. The *b*-crystallographic axis remained perpendicular to the plane of the sample and parallel to the magnetic field.

The dc isothermal magnetic field dependencies and isofield temperature dependencies were measured using a Quantum Design SQUID (superconducting quantum interference device) ac/dc susceptometer/magnetometer MPMS-XL7 and a vibrating sample magnetometer (a Quantum Design PPMS (physical properties measuring system)). The $M(H)$ measurements were carried out in external magnetic fields varying from 0 to 70 kOe. The isothermal magnetization measurements reported in this paper have been corrected for demagnetization [15]. The value of the demagnetization factor was 0.16. The accuracy of the magnetic measurements was better than 1%. In this work, long waiting periods for each temperature were implemented in order to approach a nearly ideal thermal equilibrium, and therefore, sample temperature errors were close to ± 0.1 K due to normal thermal fluctuations.

The heat capacity in constant magnetic fields (between 0 to 100 kOe) was measured from ~2 to 350 K using a semiadiabatic heat pulse calorimeter [16]. The accuracy of the heat capacity data was better than ~0.6% in the temperature interval from 20 to 350 K and better than ~1% in the 4–20 K temperature range.

3. Magnetic properties

The magnetization isotherms of the Ho single crystal measured from 5 to 20 K with the magnetic field applied parallel to the *b*-axis are shown in figure 1(*a*) for applied magnetic fields between 0 and 6 kOe (all $M(H)$ measurements were carried out in magnetic fields up to 70 kOe).

These data agree well with those reported in the literature [2, 3]. Metamagnetic-like steps in the magnetization corresponding to the magnetic-field-induced first-order AFM–FM transformation are observed at temperatures exceeding 12 K. The magnetization tends to saturate at relatively low fields (e.g. 4–6 kOe at 20 K) and is almost fully saturated at 25 kOe. The saturation value of $\sim 330\,\mathrm{emu\,g}^{-1}$ corresponds to $\sim 9.75\mu_{\mathrm{B}}$ per Ho atom, which is in a good agreement with the theoretical gJ value of $10.0\mu_{\mathrm{B}}$. Figure 1(*b*) depicts the isothermal dependencies of the magnetization for magnetic fields up to 15 kOe between 21 and 31 K. The metamagnetic behavior corresponds to the first-order transition noted in figure 1(*a*). The critical magnetic field required to induce the AFM–FM transformation gradually increases from ~2.5 to ~7.5 kOe with increasing temperature.

Magnetization curves at higher temperatures (32–65 K) are presented in figures 2(*a*) and (*b*).

The critical magnetic field required to induce the AFM–FM transformation continues to increase from ~7.5 to ~15 kOe with increasing temperature. Between 5 and 65 K only a single metamagnetic AFM–FM transition step is seen (figures 1 and 2(*b*)). A new anomaly appears as a small step in the isothermal magnetization data starting at 70 K and is clearly seen in the $M(H)$ curves up to 100 K (figure 2(*c*)). The critical field of this anomaly increases with temperature from ~16 to ~27 kOe. This anomaly is probably related to the previously reported spin–slips occurring around 95 K in

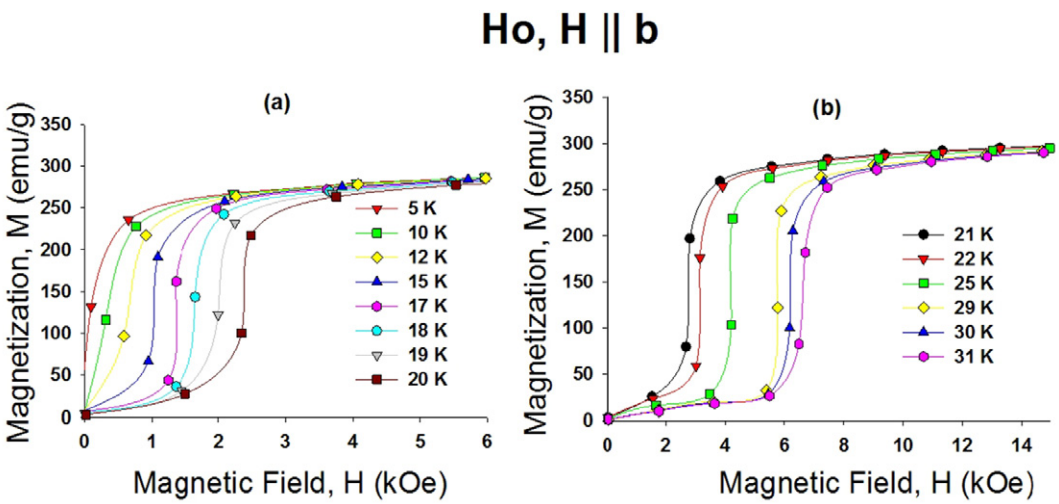

Figure 1. Isothermal magnetization of Ho measured between 5 and 20 K (*a*) and 21 and 31 K (*b*). Data are shown only from 0 to 6 kOe in (*a*) and 0 to 15 kOe for clarity. In all measurements the magnetic field vector was parallel to the *b*-axis of the crystal.

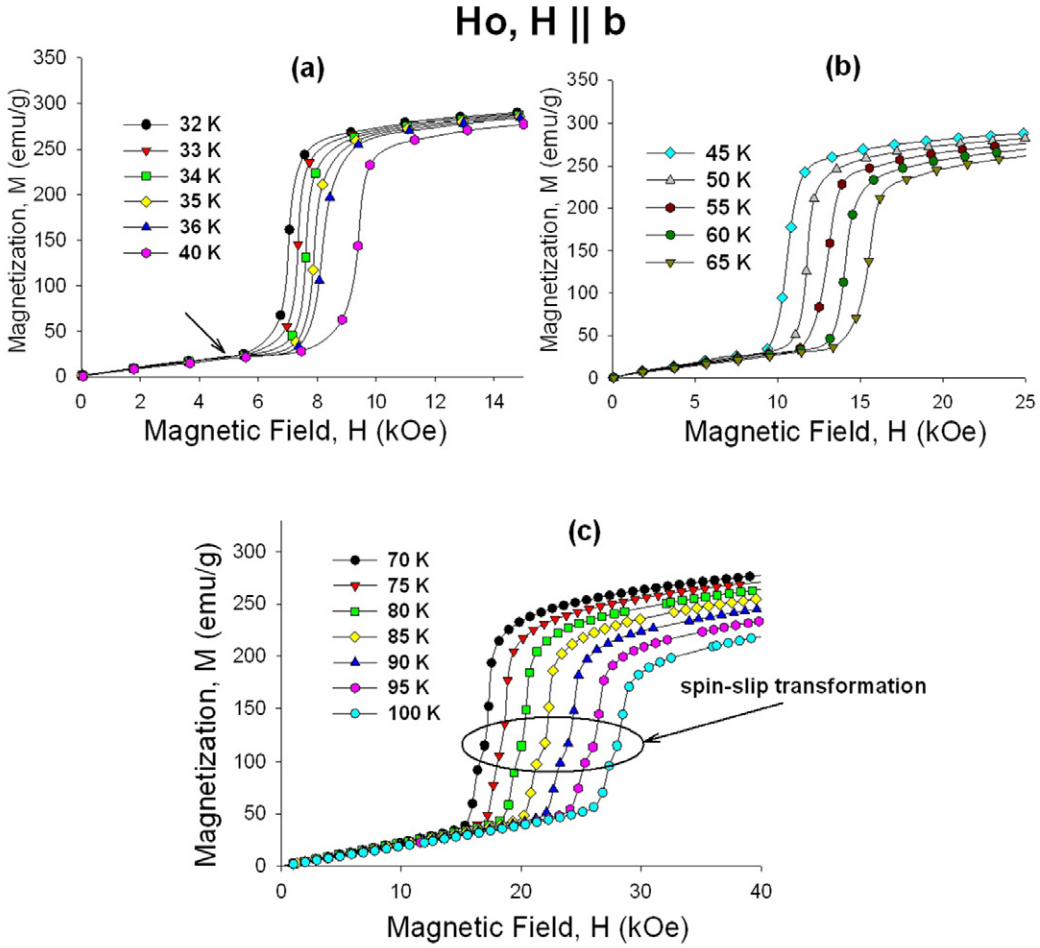

Figure 2. Isothermal magnetization of Ho measured between 32 and 40 K (*a*), 45 and 65 K (*b*), and 70 and 100 K (*c*). Only the data between 0 and 15 kOe (*a*), 0 and 25 kOe (*b*), and 0 and 40 kOe (*c*) are shown for clarity. In all measurements the magnetic field vector was parallel to the *b*-axis of the crystal.

the zero field [9]. However, the existence of this transition over a broad temperature range in applied magnetic fields has not been reported before.

$M(H)$ curves between 105 and 150 K are presented in figures 3(*a*) and (*b*).

The magnetic-field-induced anomaly connected with the spin–slip transition disappears at 105 K. The critical magnetic field of the AFM–FM transformation ($H_{cr} \sim 30$ kOe) remains practically constant at 110 and 115 K. A metamagnetic increase in the magnetization is clearly observed at 120 K at ∼27 kOe

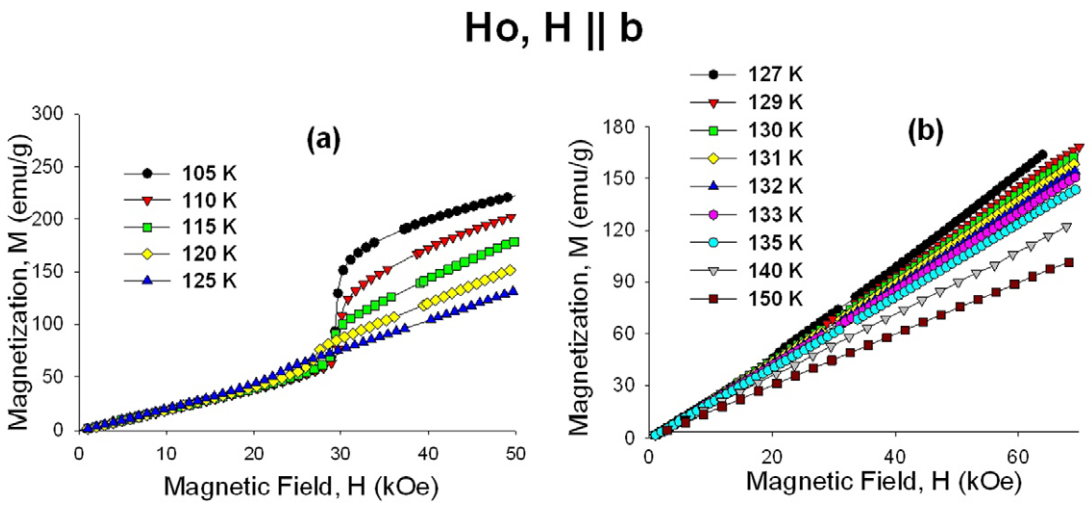

Figure 3. Isothermal magnetization of Ho measured between 105 and 125 K (*a*) and 127 and 150 K (*b*) in magnetic fields from 0 to 70 kOe. The data in (*a*) are shown between 0 and 50 kOe for clarity. In all measurements the magnetic field vector was parallel to the *b*-axis of the crystal.

but at 125 K the step in magnetization becomes nearly indistinguishable and the anomaly is reduced to a change of slope of the $M(H)$ function that occurs at progressively lower fields, i.e. ∼22 kOe at 125 K and ∼20 kOe at 127 K. At 129 K and higher temperatures the behavior of the magnetization becomes nearly linear with the field as Ho adopts the paramagnetic state.

Figure 4(*a*) shows the $M(T)$ dependence measured along the *b*-axis in a 100 Oe magnetic field. A weak anomaly is observed at ∼8 K, which likely reflects the appearance of the cone-like phase in the low field region or a transition from the cone to the ferromagnetic state. The sharp peak observed at ∼20.7 K during heating corresponds to a temperature-induced first-order FM–AFM magnetic phase transition. A cusp, seen near 130 K, corresponds to the second-order AFM–PM transition. The $M(T)$ dependencies measured on heating of the zero-field-cooled (ZFC) sample are different from those of the field-cooled (FC) sample. The value of the magnetization is higher for the FC measurements below the ferromagnetic ordering temperature. Also the temperature hysteresis (i.e. the peak ZFC and FC temperatures do not coincide), confirming the first-order character of the ∼20 K FM–AFM transition. Similar features can be seen in figure 4(*b*) where the ZFC $M(T)$ dependence measured at 500 Oe is presented. In this field the peak, which corresponds to the transition to the low-field cone-like ferromagnetic phase, is observed at ∼8 K. It is worth noting that anomalies in the FM state observed in the ZFC data measured in low fields may be related to the temperature dependent changes of coercivity, however, the fact that they are also seen in the FC data supports that these anomalies likely reflect real changes in the spin structure of the material. The temperature dependencies of the magnetization along the *b*-axis measured in 1 kOe are shown in figure 4(*c*). The behavior of the magnetization remains similar to that observed in lower fields. However, the AFM–FM transition peak at ∼ 20.7 K becomes broader, and the shape of the anomaly at 7.7 K is different.

Figure 5 shows the $M(T)$ dependencies measured in higher fields where the transition to the cone ferromagnet is suppressed. Thus one can conclude that the cone-like ferromagnetic phase exists between 0.5 and 2 kOe, which is in a good agreement with the previously published results [5]. Most of the anomalies observed in low fields (<10 kOe) below 40 K are suppressed by the magnetic field. The temperature hysteresis is no longer observed at 3 kOe and higher fields for the ZFC and the FC measured samples (FC data are not shown). All of the M versus T plots show a sharp decrease in magnetization upon heating which corresponds to the transformation of the ferromagnetic phase into another structure depending upon the magnetic field or temperature.

Weak anomalies (marked with arrows at ∼40 K and 10 kOe, and 80 K and 20 kOe) reflect the transitions to a spin–slip structure and the helifan or fan structures, respectively. The weak anomaly corresponding to the Néel temperature is observed at ∼128 K in the magnetic fields from 3–10 kOe. At 20 kOe the anomaly is slightly shifted to ∼124 K, and in a 50 kOe field the corresponding anomaly is no longer observed. However, a dM/dT plot (not shown) exhibits a sharp minimum at ∼112 K which corresponds to the Néel temperature. If one also examines the low field (100 Oe to 1 kOe) magnetization curves (figure 4), one notices an apparent shift of the AFM–PM transition temperature with increasing field from ∼130 K (100 Oe) to ∼112 K (50 kOe) which suggests that antiferromagnetic ordering is suppressed by the magnetic field. No temperature hysteresis was observed for this transition in any applied magnetic field, which confirms that the Néel point in Ho is a second-order phase transition.

4. Magnetothermal properties

The temperature dependence of the heat capacity of Ho single crystal measured in zero applied magnetic field is shown in figure 6.

Three anomalies corresponding to the Néel temperature (∼131 K), the Curie temperature 19.5 K and a spin

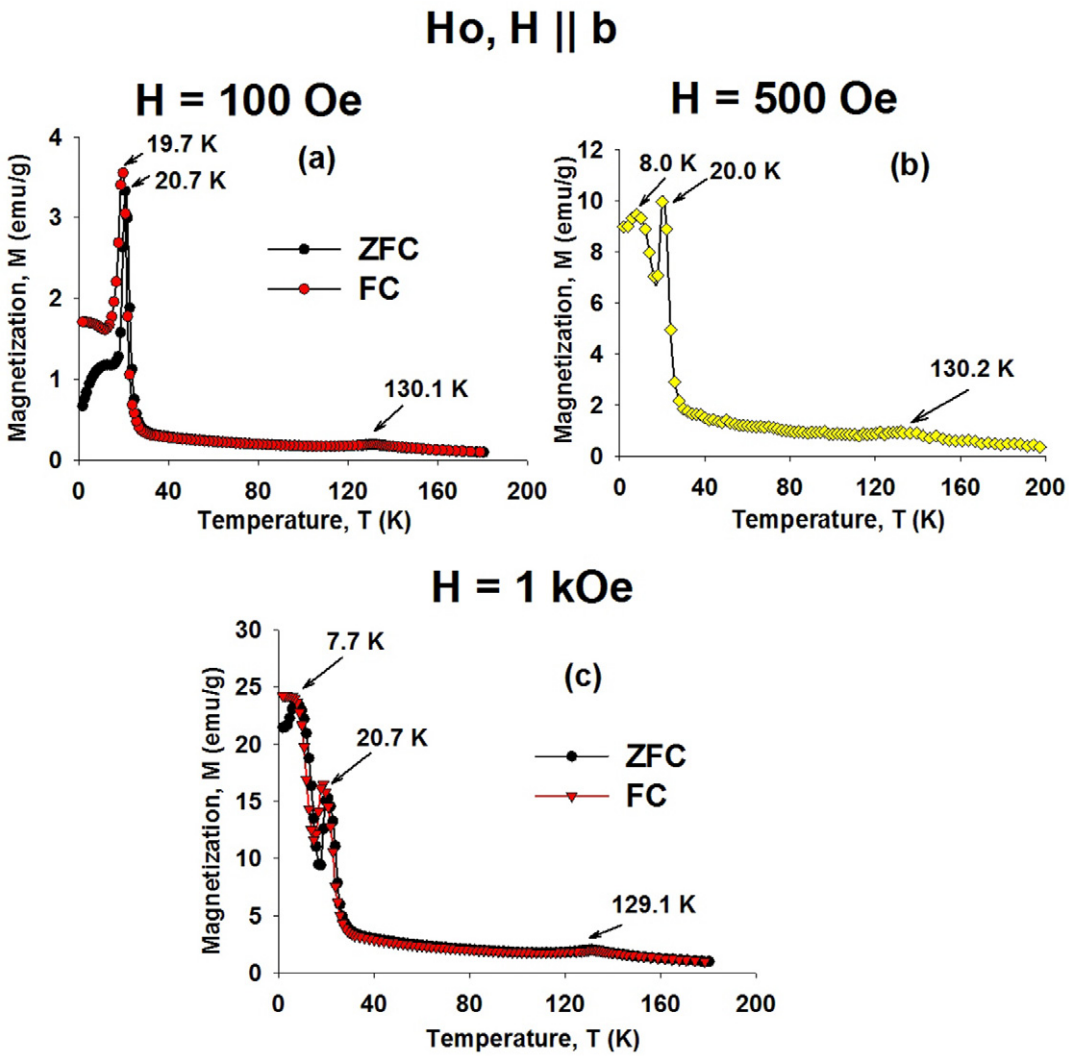

Figure 4. (*a*) Isofield magnetization of Ho measured during zero-field-cooled (ZFC) heating and field-cooled cooling from 1.5 to 180 K in a 100 Oe magnetic field parallel to the *b*-axis. (*b*) ZFC isofield magnetization of Ho measured from 1.5 to 180 K in a 500 Oe magnetic field. (*c*) Isofield magnetization of Ho measured between 1.5 and 180 K in a magnetic field of 1 kOe.

reorientation transition (17.2 K) are observed, and they are in good agreement with the results reported in the literature [4, 17, 18]. The Curie and the Néel temperatures are in full agreement with the magnetic measurements results. The anomaly at 17.2 K, which is not observed in the magnetization data, reflects the transition of one of the spin–slip structures predicted [8] to exist in Ho in this temperature region. The upturn observed below ∼4 K reflects the large nuclear specific heat of Ho [19, 20].

The temperature dependencies of the heat capacity in magnetic fields from 0 to 20 kOe applied along the *b*-axis are shown in figure 7.

The measurements were performed at 0, 2.5, 5, 7.5, 10, 12.5, 15 and 20 kOe but here we show only some of the data for clarity. A typical λ-type behavior is observed around T_N with the fields between 0 and 15 kOe. At 20 kOe a two-step behavior is observed near T_N reflecting an additional anomaly at 128 K (figure 7 inset).

The anomaly observed at 17.2 K in a zero magnetic field does not shift with increasing the field from zero to 10 kOe, but is gradually suppressed by larger applied fields. It completely disappears for $H \geqslant 12.5$ kOe (figure 8).

The 19.5 K peak (Curie temperature) observed in a zero magnetic field becomes a weak anomaly around 20 K at 2.5 and 5 kOe. This reflects the transition to the spin–slip structure as suggested by a previous study [9]. A new peak due to a metamagnet transition is observed around 27 K and is associated with a transition to the second spin–slip structure [8]. It is worth mentioning the difficulty of moving the spin slips because their interactions with the defects and the impurities in the crystal may result in the disruption of the formation of magnetic phases and a shift of the corresponding peaks. In a 20 kOe field, two peaks are observed at 32.5 K and 35.9 K, respectively (figure 8(*h*)). In order to understand the origin of the influence of the applied field on the heat capacity peak temperatures, the sample in a 20 kOe applied field was measured four times. The data were subsequently collected after cooling the sample from ∼300 K in zero magnetic field.

As shown in figure 9, the weaker peak at 32.5 K (named as the 1st peak) remained at the same temperature through the four cycles. The stronger peak at 35.9 K (named as

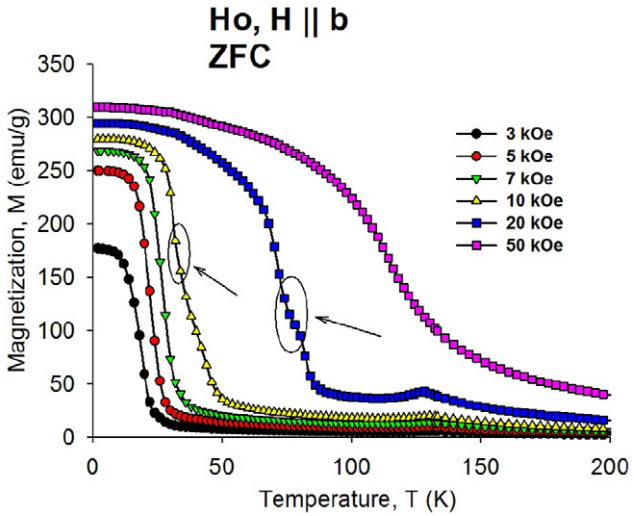

Figure 5. Isofield magnetization of Ho measured from 1.5 to 180 K along the *b*-axis in the applied magnetic fields of 3, 5, 7, 10, 20, and 50 kOe.

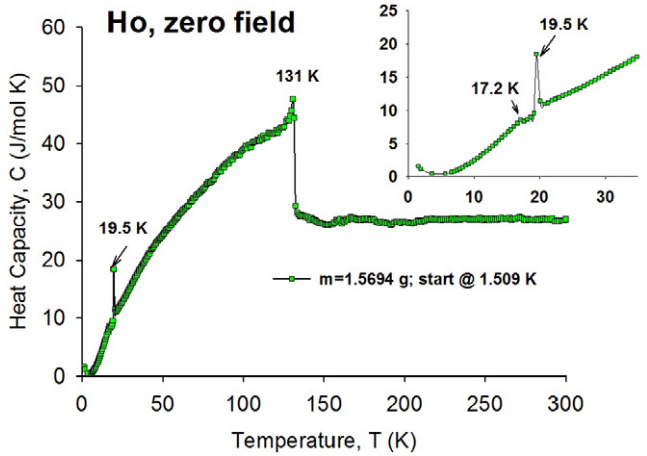

Figure 6. Temperature dependence of the heat capacity of single crystal Ho in a zero applied magnetic field. The inset shows details between 1.5 and 35 K.

the 2nd peak) gradually shifts to higher temperatures during subsequent cycles. Magnetic measurements indicate that the 1st peak corresponds to a second-order phase transition, while the 2nd peak to a first-order transition. This is in agreement with the previous studies [4, 17] which show the absence of the thermal history for the 1st peak, and the presence of the thermal history for the 2nd peak.

The heat capacity dependencies in the higher fields and temperatures do not reveal as many peaks as in the low-T region (figures 7–9). At high magnetic fields one can observe smeared anomalies probably corresponding to the transitions to the fan and ferro+fan phase in the fields up to 80 kOe (figures 9 and 10).

Analogous to the 20 kOe case (see figures 8 and 9) the two-step behavior at ∼130 K is still present in fields up to 70 kOe (figure 10(*a*)). At the same time the low T peak at ∼128 K in 2 T field K initially moves down at 30 and 40 kOe, and then moves up at 50 and 60 kOe (data not shown). The high T lambda-like transition (Néel temperature) always remains

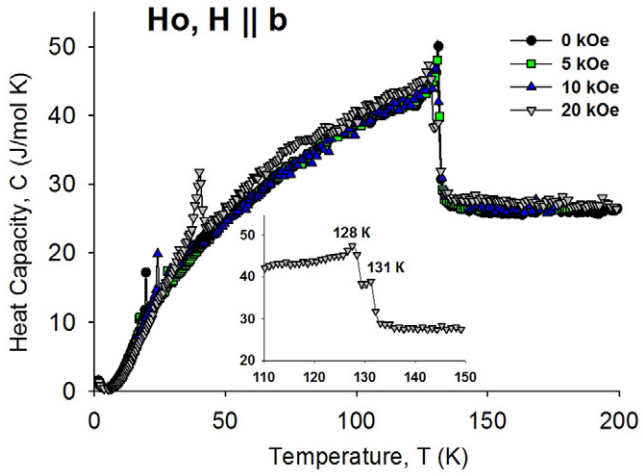

Figure 7. Temperature dependence of the heat capacity of single crystal Ho in magnetic fields between 0 and 20 kOe. The inset shows details between 110 and 150 K in a 20 kOe field.

at ∼130 K. The 30 kOe plot shows two additional peaks at ∼43 and ∼ 97 K which can be associated with the existence of the spin–slip structures. The existence of these structures in this region was supported previously by observations of slight anomalies in magnetic measurements [9]. With increasing field (figure 10(*b*)) the low T peak overlaps the discontinuity which is no longer seen at 90 kOe. Above 70 kOe the temperature of the broad Néel peak continues to increase up to 100 kOe (our highest field capability). This is the typical behavior for FM ordering in an increasing external magnetic field. Since it is rather difficult to determine the precise location of this transition in the high magnetic fields, the phase boundary on the phase diagram between the ferromagnetic and paramagnetic phases is shown as a dashed line in figure 11(*a*). The small shift of the Néel temperature to lower temperatures indicates that the magnetic field tends to suppress the AFM ordering in Ho.

5. Discussion

All of the measured physical properties of Ho show multiple temperature and magnetic-field-dependent anomalies, and they have been combined in figures 11(*a*) and (*b*), allowing us to construct the H–T phase diagram.

In general, most of the earlier published experimental results are in a good agreement with those obtained in this study. In particular, Ho behaves as a ferromagnet below the Curie temperature (T_C = 20 K) and as an antiferromagnet between the Curie and Néel temperatures (T_N = 131 K) in magnetic fields from zero to ∼30 kOe. The anomalies associated with the presence of the cone structure along the hard c-direction at low fields (up to 1 kOe) and low temperatures (below 20 K) have also been included in figures 11(*a*) and (*b*). We also detected anomalies, which are associated with the intermediate helifan and fan phases during the field induced transition from the AFM state to the FM state. The nature of the observed helifan cannot be determined by simple magnetic measurements, and a neutron

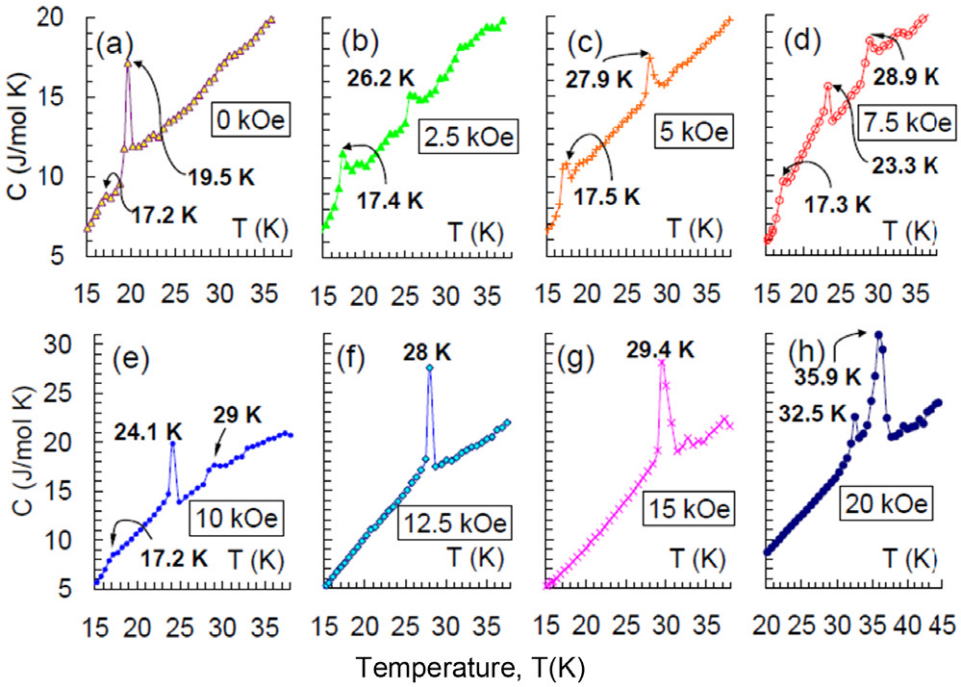

Figure 8. Panels (*a*)–(*g*) show the heat capacity of Ho between 15 and 38 K and in applied magnetic fields ranging from 0 to 15 kOe. Panel (*h*) shows the heat capacity of Ho between 20 and 45 K in a 20 kOe field.

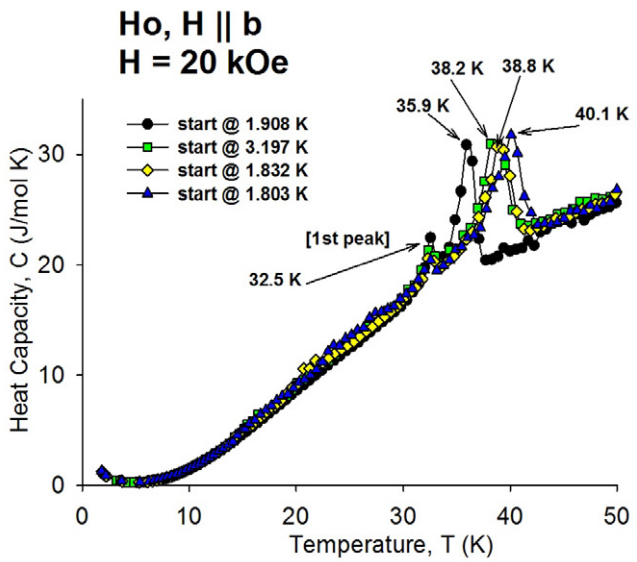

Figure 9. Temperature dependencies of the heat capacity of single crystal Ho in the 20 kOe applied magnetic field between 0 and 50 K measured after cooling in zero magnetic field for various starting temperatures.

diffraction study is required to determine its exact structure. The two-phase region between the fan and FM phases has been also observed in magnetoresistance measurements [7]. In comparison with the five intermediate phases reported by Akhavan and Blackstead [7] we have found just one. Since it is impossible to compare the chemical purity of the samples used by Akhavan and Blackstead and our samples (no data was given in [7]) we cannot discuss the influence of impurities on the phase diagram. We suggest that specific impurity(ies) and amounts thereof, may account for some mixed state(s) in Ho. It is also worth mentioning that the presence or absence of the crystalline defects may play a significant role in forming metastable magnetic phases combining the features of various magnetic orderings. At temperatures above 131.7 K Ho is paramagnetic at all fields up to 100 kOe.

The magnetic phase region between ~95 K and the Néel temperature and magnetic fields between 30 and 100 kOe is presumably associated with the transition to the commensurate spin–slip structure, the signature of which has been observed at 98 K in magnetization curves by Ali *et al* [9]. However the precise boundaries of this structure's existence in Ho had not been determined by Ali *et al* [9].

Figure 11(*b*) shows the phase relationships in the Ho phase diagram in magnetic fields from 0 to 30 kOe. Two spin–slip regions exist between 20 and 35 K (I) and between 35 and 42 K (II). The occurrence of the spin–slip transformations had been reported in these temperature intervals [8, 9]. Even though the existence of these structures has been observed previously, we have verified their existence by employing various types of measurements (field and temperature dependencies of magnetization, and heat capacity); earlier workers used only one experimental technique. In addition we have also determined the magnetic field intervals over which these phase transformations exist. Outside the temperature range from 19 to 131 K (below the Néel temperature) and in the field interval from 10 to 80 kOe Ho is a pure ferromagnet (the area is marked with 'FM' in the phase diagram).

6. Conclusion

Detailed heat capacity and magnetization measurements of a high purity (99.92 at.%) Ho single crystal in magnetic fields

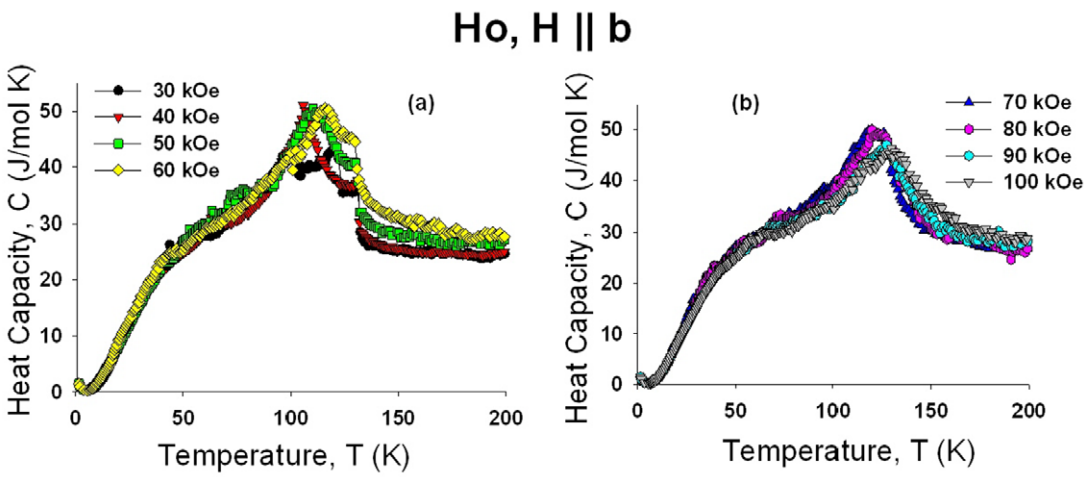

Figure 10. Temperature dependence of the heat capacity of Ho in magnetic fields between 30 and 60 kOe (*a*) and between 70 and 100 kOe (*b*). In all measurements the magnetic field vector was parallel to the *b*-axis of the crystal.

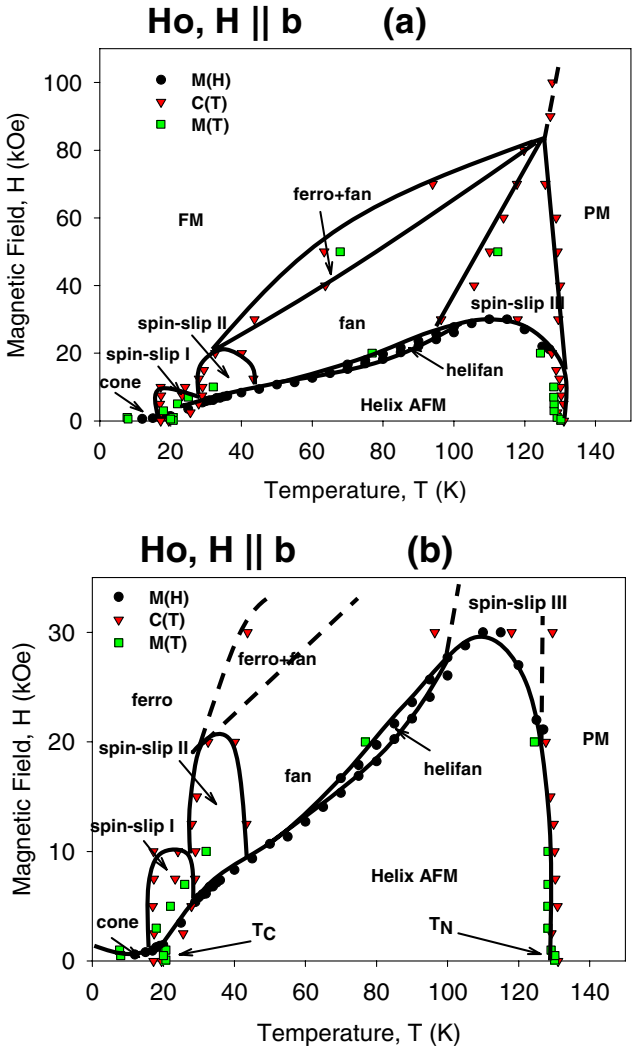

Figure 11. The magnetic phase diagram of single crystalline Ho with the magnetic field vector parallel to the easy magnetization direction (*b*-axis). Panel (*a*) shows the temperature range between 0 and 150 K and magnetic field between 0 and 100 kOe. Panel (*b*) shows details in fields lower than 35 kOe.

from 0 to 100 kOe applied parallel to the *b*-axis have been carried out from 1.5 to 350 K. These measurements led to the refinement of the magnetic phase diagram of Ho. Together with the already known phases such as the helical AFM phase between 20 and 131 K and the ferromagnetic cone type structure observed below 20 K in low magnetic fields, we observed three regions of spin–slip structures in the intervals 20–35, 35–42, and 95–110 K. The boundaries of the spin–slip structures have been clarified. The existence of 'spin–slip III' is broader than reported in previous studies. In addition to the known helifan and fan phases observed in Ho, we observed another phase of the 'ferro+fan' type, which is located between 40–120 K and 20–80 kOe.

Acknowledgments

Work at the Ames Laboratory is supported by the Office of Basic Energy Sciences, Materials Sciences Division of the Office of Science of the US Department of Energy, under contract No. DE-AC02-07CH11358 with Iowa State University (ZM, YaM, VKP and KAG). Work in Advanced Magnetic Technologies and Consulting LLC and Pharmag LLC is supported by Skolkovo Foundation, Russia.

References

[1] Jensen J and Mackintosh A R 1991 *Rare Earth Magnetism: Structure and Excitations* (Oxford: Clarendon)
[2] Rhodes B L, Legvold S and Spedding F H 1958 *Phys. Rev.* **109** 1547
[3] Strandberg D L, Legvold S and Spedding F H 1962 *Phys. Rev.* **127** 2046
[4] Gerstein B C, Griffel M, Jennings L D and Miller R E 1957 *J. Chem. Phys.* **27** 394
[5] Koehler W C, Cable J W, Wilkinson M K and Wollan E O 1966 *Phys. Rev.* **151** 414
[6] Koehler W C, Cable J W, Child H R, Wilkinson M K and Wollan E O 1967 *Phys. Rev.* **158** 450

[7] Akhavan M and Blackstead H A 1976 *Phys. Rev.* B **13** 1209
[8] Cowley R A and Bates S 1988 *J. Phys. C: Solid State Phys.* **21** 4113
[9] Ali N, Willis F, Steinitz M O, Kahrizi M and Tindall D A 1989 *Phys. Rev.* B **40** 11414
[10] Hughes I D, Daene M, Ernst A, Hergert W, Lueders M, Staunton J B, Svane A, Szotek Z and Temmerman W M 2007 *Nat. Lett.* **446** 650
[11] Mackintosh A R and Jensen J 1992 *J. Magn. Magn. Mater.* **104–107** 1481
[12] Gschneidner K A Jr 1993 *J. Alloys Compd* **193** 1
[13] Materials Preparation Center, Ames Laboratory of US Department of Energy, Ames, IA (www.mpc.ameslab.gov)
[14] Gschneidner K A Jr and Daane A H 1988 *Handbook on the Physics and Chemistry of Rare Earths* vol 11, ed K A Gschneidner Jr and L Eyring (Amsterdam: Elsevier)
[15] Chen D X, Pardo E and Sanchez A 2002 *IEEE Trans. Magn.* **38** 1742
[16] Pecharsky V K, Moorman J O and Gschneidner K A Jr 1997 *Rev. Sci. Instrum.* **68** 4196
[17] Lounasmaa O V and Sundstroem L J 1966 *Phys. Rev.* **150** 399
[18] Lounasmaa O V 1962 *Phys. Rev.* **128** 1136
[19] Krusius M, Anderson A C and Holmstroem B 1969 *Phys. Rev.* **177** 910
[20] Gordon J E, Dempesy C W and Soller T 1961 *Phys. Rev.* **124** 724